

DTIC FILE COPY

4

AD-A197 875

TECHNICAL REPORT BRL-TR-2931

(SUPERSEDES IMR-0899)

BRL

1938 - Serving the Army for Fifty Years - 1988

COMPUTATION OF THE ROLL CHARACTERISTICS
OF FINNED PROJECTILESPAUL WEINACHT
WALTER B. STUREK

JUNE 1988

DTIC
ELECTE
AUG 08 1988
S H D

APPROVED FOR PUBLIC RELEASE; DISTRIBUTION UNLIMITED.

U.S. ARMY LABORATORY COMMAND

BALLISTIC RESEARCH LABORATORY
ABERDEEN PROVING GROUND, MARYLAND

DESTRUCTION NOTICE

Destroy this report when it is no longer needed. DO NOT return it to the originator.

Additional copies of this report may be obtained from the National Technical Information Service, U.S. Department of Commerce, Springfield, VA 22161.

The findings of this report are not to be construed as an official Department of the Army position, unless so designated by other authorized documents.

The use of trade names or manufacturers' names in this report does not constitute indorsement of any commercial product.

UNCLASSIFIED

SECURITY CLASSIFICATION OF THIS PAGE

REPORT DOCUMENTATION PAGE				Form Approved OMB No. 0704-0188		
1a. REPORT SECURITY CLASSIFICATION UNCLASSIFIED			1b. RESTRICTIVE MARKINGS			
2a. SECURITY CLASSIFICATION AUTHORITY			3. DISTRIBUTION/AVAILABILITY OF REPORT Approved for public release, distribution unlimited.			
2b. DECLASSIFICATION/DOWNGRADING SCHEDULE						
4. PERFORMING ORGANIZATION REPORT NUMBER(S) BRL-TR-2931			5. MONITORING ORGANIZATION REPORT NUMBER(S)			
6a. NAME OF PERFORMING ORGANIZATION U.S. Army Ballistic Research Laboratory		6b. OFFICE SYMBOL (if applicable) SLCBBR-LF	7a. NAME OF MONITORING ORGANIZATION			
6c. ADDRESS (City, State, and ZIP Code) Aberdeen Proving Ground, Maryland 21005-5066			7b. ADDRESS (City, State, and ZIP Code)			
8a. NAME OF FUNDING/SPONSORING ORGANIZATION		8b. OFFICE SYMBOL (if applicable)	9. PROCUREMENT INSTRUMENT IDENTIFICATION NUMBER			
8c. ADDRESS (City, State, and ZIP Code)			10. SOURCE OF FUNDING NUMBERS			
			PROGRAM ELEMENT NO. 62618A	PROJECT NO. 1L162618AH80	TASK NO. 00	WORK UNIT ACCESSION NO. 00
11. TITLE (Include Security Classification) COMPUTATION OF THE ROLL CHARACTERISTICS OF FINNED PROJECTILES						
12. PERSONAL AUTHOR(S) WEINACHT, PAUL and STUREK, WALTER B.						
13a. TYPE OF REPORT Technical Report		13b. TIME COVERED FROM _____ TO _____		14. DATE OF REPORT (Year, Month, Day)		
15. PAGE COUNT						
16. SUPPLEMENTARY NOTATION						
17. COSATI CODES			18. SUBJECT TERMS (Continue on reverse if necessary and identify by block number)			
FIELD 01	GROUP 02	SUB-GROUP	Kinetic Energy Projectiles			
01	04		Parabolized Navier-Stokes			
			Finned Projectiles			
			Roll Damping			
			Roll Characteristics			
			Computational Fluid Dynamics			
19. ABSTRACT (Continue on reverse if necessary and identify by block number) The Computational Aerodynamics Branch, Launch and Flight Division has been actively developing the capability to predict the aerodynamics of US Army projectiles using Computational Fluid Dynamics (CFD) techniques. Currently under development is the capability to predict the supersonic aerodynamics of finned projectiles such as kinetic energy (KE) penetrators. In the current research effort, several important aerodynamic parameters which influence the roll characteristics of a fielded kinetic energy projectile (M735) have been predicted using CFD techniques. These parameters include the roll producing moment (at zero spin rate), the roll damping moment, and the equilibrium spin rate, defined as the spin rate for which the net roll moment is zero. Viscous CFD computations have been performed over a range of Mach numbers and spin rates using the US Army's Cray-2 supercomputer located at the Ballistic Research Laboratory. The computed results have been used to benchmark and validate engineering approaches for computing these aerodynamic coefficients.						
20. DISTRIBUTION/AVAILABILITY OF ABSTRACT <input checked="" type="checkbox"/> UNCLASSIFIED/UNLIMITED <input type="checkbox"/> SAME AS RPT. <input type="checkbox"/> DTIC USERS			21. ABSTRACT SECURITY CLASSIFICATION UNCLASSIFIED			
22a. NAME OF RESPONSIBLE INDIVIDUAL Paul Weinacht			22b. TELEPHONE (Include Area Code) (301) 278-4280		22c. OFFICE SYMBOL SLCBBR-LF-R	

TABLE OF CONTENTS

	<u>Page</u>
LIST OF FIGURES.....	v
I. INTRODUCTION.....	1
II. GOVERNING EQUATIONS AND COMPUTATIONAL TECHNIQUE.....	2
1. THIN-LAYER NAVIER-STOKES EQUATIONS.....	2
2. THE PARABOLIZED NAVIER-STOKES (PNS) PROCEDURE.....	5
3. INVISCID SPACE-MARCHING PROCEDURE.....	6
III. ENGINEERING ESTIMATION OF THE ROLL CHARACTERISTICS.....	6
1. ESTIMATION OF THE ROLL PRODUCING MOMENT.....	6
a. Trailing edge.....	6
b. Leading edge.....	7
2. ESTIMATION OF THE ROLL DAMPING OF A KE FIN.....	7
IV. RESULTS.....	8
1. ROLL PRODUCING MOMENT.....	9
2. ROLL MOMENT ON A SPINNING PROJECTILE.....	10
3. TRAJECTORY SIMULATION.....	10
V. CONCLUSION.....	11
REFERENCES.....	27
LIST OF SYMBOLS.....	29
DISTRIBUTION LIST.....	31

Q111
INSPECTED
2

Accession For	
NTIS GRA&I	<input checked="" type="checkbox"/>
DTIC TAB	<input type="checkbox"/>
Unannounced	<input type="checkbox"/>
Justification	
By	
Distribution/	
Availability Codes	
Dist	Avail and/or Special
A-1	

LIST OF FIGURES

<u>Figure</u>		<u>Page</u>
1	Schematic of M735 finned projectile geometry.....	12
2	Schematic of M735 fin cross-sectional geometry.....	13
3	Development of roll producing moment coefficient with axial position, $M = 3$, $pD/V = 0$	14
4	Variation of roll producing moment coefficient with Mach number..	15
5a	Pressure difference across fin near trailing edge, Sections 1-7, inviscid result.....	16
5b	Pressure difference across fin near trailing edge, Sections 1-7, viscous result.....	17
6	Schematic showing spanwise location of pressure profiles.....	18
7	Mach contours in vicinity of trailing edge, $M = 3$, $pD/V = 0$	19
8	Development of net roll moment coefficient with axial position, $M = 3$, $pD/V = 0.008568$	20
9	Variation of net roll moment coefficient with spin rate, $M = 3.0$	21
10	Variation of roll damping coefficient with Mach number.....	22
11	Variation of non-dimensional equilibrium spin rate with Mach number.....	23
12	Variation of dimensional equilibrium spin rate with Mach number..	24
13	Roll rate history from trajectory simulation using computed and estimated roll coefficients.....	25
14	Comparison of spin rate versus Mach number for equilibrium spin rate and trajectory simulation.....	26

I. INTRODUCTION

The Computational Aerodynamics Branch, Launch and Flight Division has been actively developing the capability to predict the aerodynamics of US Army projectiles using Computational Fluid Dynamics (CFD) techniques. Successful prediction of Magnus force for a spinning artillery projectile at supersonic velocities is a prime example of the powerful nature of these techniques.^{1,2} The eventual goal of CFD techniques is to allow the projectile designer to compute the flow field about given projectile designs accurately and efficiently resulting in improved performance of future projectile designs.

Currently under development is the capability to predict the supersonic aerodynamics of finned missiles such as kinetic energy (KE) penetrators.^{3,4} Kinetic energy penetrators are long length-to-diameter ratio finned projectiles which are used to defeat armored targets by punching holes through the armor. Previous efforts have focused on computing the pitch-plane aerodynamics of these projectiles. In this report, several important aerodynamic parameters which influence the roll characteristics of a fielded kinetic energy projectile (M735) have been predicted using CFD techniques. These parameters include the roll producing moment (at zero spin rate), the roll damping moment, and the equilibrium spin rate, defined as the spin rate for which the net roll moment is zero.

In contrast to conventional spin-stabilized shell configurations, KE penetrators rely on fins to remain aerodynamically stable, although these projectiles fly with small spin rates to decrease the dispersion of the round. The spin on the projectile results from the aerodynamic loads produced by the machined asymmetries in the fin geometry. The geometry of the M735 KE projectile is shown in Figures 1 and 2. The asymmetries in the fin geometry at the leading and trailing edges of the fins are typical of kinetic energy projectiles.

KE penetrators can be launched from either smooth-bore or rifled gun tubes. In the case of the smooth-bore gun, the projectile is launched with an initial spin rate which is nearly zero and rolls up to a spin rate which is nearly constant throughout the later stages of the trajectory. Penetrators launched from a rifled gun tube (with a slip-ring sabot) often have an initial spin rate higher than the equilibrium spin rate and roll down to a nearly constant value. Aero-ballisticians describe the spin history in terms of the following ordinary differential equation;⁵

$$I \frac{dp}{dt} = (1/2) \rho_{\infty} a_{\infty}^2 M_{\infty}^2 D S_{ref} C_l \quad (1)$$

where p is the spin rate, t is time, I is the moment of inertia, and C_l is the net aerodynamic roll moment acting on the projectile, and ρ_{∞} , a_{∞} , M_{∞} , D and S_{ref} are respectively the reference density, speed of sound, Mach number, diameter, and area.

The net aerodynamic roll moment is composed of two components, the roll producing moment resulting from the aerodynamic loads produced by the machined asymmetries in the fin geometry which tends to induce spin, and the roll

damping contribution which consists of pressure and viscous forces that oppose the spin. The relationship of these contributions to the net aerodynamic roll moment is expressed below in non-dimensional form,

$$C_{\ell} = C_{\ell_0} - C_{\ell_p} \frac{pD}{V} \quad (2)$$

where C_{ℓ_0} is the roll producing moment coefficient, C_{ℓ_p} is the roll damping moment coefficient and pD/V is the non-dimensional spin rate.

As is suggested by Equation (2), the roll producing moment can be obtained by computing the net roll moment at zero spin rate, while roll damping moment is obtained by computing the net roll moment on the projectile at a fixed spin rate, and subtracting it from the roll producing moment and dividing by the spin rate. The equilibrium spin rate, which occurs when the net aerodynamic roll moment is zero, is obtained by dividing the roll producing moment by the roll damping moment.

In this report, the net aerodynamic roll moment is obtained by computing the flow field around the projectile using CFD techniques. The techniques applied in this report are described in the following section. Engineering approaches for determining the roll characteristics are also briefly described and are compared with the computed results.

II. GOVERNING EQUATIONS AND COMPUTATIONAL TECHNIQUE

Computation of the viscous flow field about the finned projectile configuration is accomplished by solving the thin-layer Navier-Stokes equations using the Parabolized Navier-Stokes technique. The computations have been performed at zero degrees angle of attack in a rotating coordinate frame which rotates at the spin rate of the projectile. Performing the computations in rotating coordinate frame allows the time-independent or steady-state governing equations to be solved, at a significantly reduced computational cost compared with computations performed in the traditional space fixed coordinate frame.

Additional cost savings are achieved by performing the computations in cylindrical coordinates to take advantage of the periodic symmetry of the current configuration of interest. Over the cylindrical portion of the body, the flow field is completely symmetric in the circumferential direction, while over the finned portion of the body, the solution is symmetric with a period of 60 degrees, due to the symmetric arrangement of the six fins.

1. THIN-LAYER NAVIER-STOKES EQUATIONS

The set of equations that describes three-dimensional compressible viscous flow is referred to as the Navier-Stokes equations. The Navier-Stokes equations express the conservation of mass, momentum, and energy in the three coordinate directions. The thin-layer Navier-Stokes equations, which are solved in this report, are obtained by eliminating from the full Navier-Stokes equations, all the viscous terms except for those containing derivatives in

the direction nearly normal to the projectile body. For high Reynolds number flows with no axial flow separation, the thin-layer Navier-Stokes equations are a very good approximation to the full Navier-Stokes equations, and can be efficiently solved using available numerical algorithms.

The Reynolds averaged thin-layer Navier-Stokes equations, cast in generalized cylindrical coordinates and containing the rotating coordinate frame terms, are shown below.

$$\frac{\partial E}{\partial \xi} + \frac{\partial F}{\partial \eta} + \frac{\partial G}{\partial \zeta} + S + H = \frac{\partial G_v}{\partial \zeta} + S_v \quad (3)$$

Here, E, F and G are the inviscid flux vectors, G_v is the viscous flux vector, S and S_v are the inviscid and viscous source terms due to the cylindrical coordinate formulation, and H is the source term containing the Coriolis and centrifugal force terms which result from the rotating coordinate frame. Each of these matrices are functions of the dependent variables represented by the vector, $q(\rho, \rho u, \rho v, \rho w, e)$, where ρ is the density, u, v, w, are the velocity components in the three spacial directions x, θ , and r, and e is the total energy per unit volume. Each of flux vectors and source terms are defined below.

$$E = \frac{1}{J} \begin{bmatrix} \rho U \\ \rho u U + \xi_x P \\ \rho v U \\ \rho w U \\ (e + P)U \end{bmatrix}$$

$$F = \frac{1}{J} \begin{bmatrix} \rho V \\ \rho u V + \eta_x P \\ \rho v V + \eta_\theta P/r \\ \rho w V + \eta_r P \\ (e + P)V \end{bmatrix}$$

$$G = \frac{1}{J} \begin{bmatrix} \rho W \\ \rho u W + \zeta_x P \\ \rho v W + \zeta_\theta P/r \\ \rho w W + \zeta_r P \\ (e + P)W \end{bmatrix}$$

$$S = \frac{1}{Jr} \begin{bmatrix} \rho W \\ \rho u W \\ 2\rho v W \\ \rho(w^2 - v^2) \\ (e + P)W \end{bmatrix}$$

$$G_v = \frac{1}{J} \begin{bmatrix} 0 \\ m_1 \frac{\partial u}{\partial \zeta} + m_2 \zeta_x \\ m_1 \frac{\partial v}{\partial \zeta} + m_2 \zeta_\theta / r \\ m_1 \frac{\partial w}{\partial \zeta} + m_2 \zeta_r \\ m_3 \end{bmatrix}$$

$$H = \frac{1}{J} \begin{bmatrix} 0 \\ 0 \\ 2\Omega \rho w \\ -2\Omega \rho v - \Omega^2 r \rho \\ -\Omega^2 r \rho v \end{bmatrix}$$

$$\begin{aligned}
& 0 \\
& - \zeta_x \frac{\partial}{\partial \zeta} \left((\mu + \mu_t) \frac{2w}{3r} \right) + \frac{(\mu + \mu_t)}{r} \left(\zeta_r \frac{\partial u}{\partial \zeta} + \zeta_x \frac{\partial w}{\partial \zeta} \right) \\
& - \zeta_r \frac{\partial}{\partial \zeta} \left((\mu + \mu_t) \frac{v}{r} \right) + \frac{1}{r} \zeta_\theta \frac{\partial}{\partial \zeta} \left((\mu + \mu_t) \frac{4w}{3r} \right) \\
& + \frac{2(\mu + \mu_t)}{r} \left(\frac{1}{r} \zeta_\theta \frac{\partial w}{\partial \zeta} + \zeta_r \frac{\partial v}{\partial \zeta} - \frac{v}{r} \right) \\
& - \frac{1}{r} \zeta_\theta \frac{\partial}{\partial \zeta} \left((\mu + \mu_t) \frac{v}{r} \right) - \zeta_r \frac{\partial}{\partial \zeta} \left((\mu + \mu_t) \frac{2w}{3r} \right) \\
& + \frac{2(\mu + \mu_t)}{r} \left(\frac{-1}{r} \zeta_\theta \frac{\partial v}{\partial \zeta} + \zeta_r \frac{\partial w}{\partial \zeta} - \frac{w}{r} \right) \\
& - \zeta_x \frac{\partial}{\partial \zeta} \left((\mu + \mu_t) \frac{2uw}{3r} \right) + \frac{1}{r} \zeta_\theta \frac{\partial}{\partial \zeta} \left((\mu + \mu_t) \frac{vw}{3r} \right) \\
& - \frac{1}{r} \zeta_r \frac{\partial}{\partial \zeta} \left((\mu + \mu_t) \left(v^2 + \frac{2w^2}{3} \right) \right) + \frac{1}{2r} (\mu + \mu_t) \zeta_r \frac{\partial}{\partial \zeta} (q^2) \\
& - \frac{2w}{3r} (\mu + \mu_t) \left(\zeta_x \frac{\partial u}{\partial \zeta} + \frac{1}{r} \zeta_\theta \frac{\partial v}{\partial \zeta} + \zeta_r \frac{\partial w}{\partial \zeta} \right) \\
& + \frac{1}{r} (\mu + \mu_t) \left(u \zeta_x \frac{\partial w}{\partial \zeta} + \frac{1}{r} v \zeta_\theta \frac{\partial w}{\partial \zeta} + w \zeta_r \frac{\partial w}{\partial \zeta} \right) \\
& + \frac{1}{(\gamma - 1)} \left(\frac{\mu}{pr} + \frac{\mu_t}{pr_t} \right) \zeta_r \frac{\partial}{\partial \zeta} (a^2)
\end{aligned}
\tag{4}$$

where the contravariant velocity components are defined:

$$U = u \xi_x$$

$$V = u \eta_x + v \eta_\theta / r + w \eta_r$$

$$W = u \zeta_x + v \zeta_\theta / r + w \zeta_r$$

and the metric quantities are defined

$$\xi_x = \frac{1}{x_\xi}$$

$$\eta_x = J(r_\xi \theta_\zeta - \theta_\xi r_\zeta) \quad , \quad \eta_\theta = J(x_\xi r_\zeta) \quad , \quad \eta_r = J(-x_\xi \theta_\zeta)$$

$$\zeta_x = J(\theta_\xi r_\eta - r_\xi \theta_\eta) \quad , \quad \zeta_\theta = J(-x_\xi r_\eta) \quad , \quad \zeta_r = J(x_\xi \theta_\eta)$$

and where

$$m_1 = (\mu + \mu_t)(\zeta_x^2 + (\zeta_\theta/r)^2 + \zeta_r^2)$$

$$m_2 = \frac{1}{3}(\mu + \mu_t) \left(\zeta_x \frac{\partial u}{\partial \zeta} + \frac{1}{r} \zeta_\theta \frac{\partial v}{\partial \zeta} + \zeta_r \frac{\partial w}{\partial \zeta} \right)$$

$$m_3 = \frac{1}{(\gamma - 1)} \left(\frac{\mu}{Pr} + \frac{\mu_t}{Pr_t} \right) \left(\zeta_x^2 + (\zeta_\theta/r)^2 + \zeta_r^2 \right) \frac{\partial}{\partial \zeta} (a^2) + \frac{1}{2} m_1 \frac{\partial}{\partial \zeta} (q^2) \\ + m_2 \left(u \zeta_x + \frac{v}{r} \zeta_\theta + w \zeta_r \right)$$

$$a^2 = \frac{\gamma P}{\rho}$$

$$q^2 = u^2 + v^2 + w^2$$

Closure of this set of equations is obtained by applying the ideal gas law, which allows the pressure to be related to the dependent variables in the following manner.

$$P = (\gamma - 1)[e - (\rho/2)q^2] \quad (5)$$

The turbulent viscosity, μ_t , which appears in the viscous matrices is computed using the Baldwin-Lomax turbulence model.⁶

2. THE PARABOLIZED NAVIER-STOKES (PNS) PROCEDURE

The Parabolized Navier-Stokes (PNS) technique of Schiff and Steger⁷ is widely used to compute the supersonic viscous flow about variety of flight vehicles by solving the steady thin-layer Navier-Stokes equations using a procedure which allows the solution to be spacially marched along the body in the main flow direction due to the parabolic nature of the governing

equations. An initial plane of data is required to begin the space marching procedure and may be obtained either from an auxiliary calculation or from a conical starting procedure, as has been done for the results presented here. Following the approach of Schiff and Steger,⁷ the governing equations, which have been modified to include the Coriolis and centrifugal force terms, are solved using a conservative, approximately factored, implicit finite-difference numerical algorithm as formulated by Beam and Warming.⁸ In the results presented here capturing of the bow shock has been performed. Further details of the procedure are readily available in the literature.

For the computational results presented here, the grid consisted of 60 points from the body to the outer boundary. In the circumferential direction, the gridding was performed over a 60 degree arc due to the periodic symmetry present in the configuration of interest. Over the axisymmetric portion of the body, six circumferential points were used. (This was somewhat arbitrary since the flow is axisymmetric over the body.) On the finned portion of the body, 50 circumferential points were used to span the 60 degree arc.

Starting solutions were obtained using the conical step-back procedure. For each Mach number, starting solutions for the non-spinning case were typically obtained in 360 seconds on a Cray-2 supercomputer. Starting solutions for each additional spin rate were generated by re-converging the non-spinning starting solution and typically required an additional 100 seconds. Marching the solution over the cylindrical portion of the body and the fins required 100 seconds and 750 seconds, respectively.

Solutions were obtained over the full circumferential plane (360 degrees) to check the implementation of the periodic boundary conditions. The results were essentially identical to the periodic results and required about five times more CPU time. A grid refinement study was also performed by doubling the grid points in the circumferential direction. The results showed only a 1.5 percent variation in the roll producing moment at Mach 3.

3. INVISCID SPACE-MARCHING PROCEDURE

The viscous results have been supplemented by inviscid computations. The inviscid procedure applied here is based on the PNS procedure except that the viscous terms have been eliminated, viscous sublayer approximation ignored, and appropriate boundary conditions have been applied at the projectile surface. Inviscid results have only been obtained for zero spin rate.

III. ENGINEERING ESTIMATION OF THE ROLL CHARACTERISTICS

1. ESTIMATION OF THE ROLL PRODUCING MOMENT

The roll producing moment caused by the machined asymmetries on the fin can be estimated using simple compressible flow theories. Asymmetries exist at both the leading and trailing edges of the fins, and the contributions of each to the roll producing moment are discussed in the following sections.

a. Trailing edge The trailing edge of the fin is machined at a constant slope of seven degrees as shown in Figure 2. This region can be treated as an inverted wedge and the equations for Prandtl Meyer flow can be applied to

compute the pressure difference across the trailing edge bevel, which is constant under the assumption of two-dimensional flow. The roll producing moment can be computed from the pressure difference as shown below

$$C_{\ell_0} = \frac{N_{fins}(\Delta P/P_\infty)AZ}{\frac{1}{2} \gamma M_\infty^2} \quad (6)$$

where A is the area of the trailing edge bevel, Z is the moment arm from the projectile axis to the centroid of the beveled area, γ is the ratio of specific heats, M_∞ is the free stream Mach number, P_∞ is the free stream static pressure, ΔP is the pressure difference across the beveled trailing edge, and N_{fins} is the number of fins.

By assuming free stream conditions in front of the trailing edge bevel and on the non-beveled side of the fin, the Prandtl-Meyer equations can be applied to compute the pressure difference across the fin. These relations are available in standard compressible flow texts such as Reference 9.

b. Leading edge The leading edge of the fin for some KE projectiles may have an asymmetric leading edge which can contribute to the roll producing moment. Estimates of this contribution to the roll producing moment can be obtained by treating the leading edge chamfer as a two-dimensional wedge. This component of the roll producing moment can be estimated as follows,

$$C_{\ell_0} = \frac{N_{fins}((P_R/P_\infty - 1)A_R Y_R - (P_L/P_\infty - 1)A_L Y_L)}{\frac{1}{2} \gamma M_\infty^2} \quad (7)$$

where P_R and P_L are the pressures on the right and left faces of the leading edge chamfer, A_R and A_L are the areas of the leading edge chamfers, Y_R and Y_L are the locations of the centroids of the areas. The pressures P_R and P_L can be obtained by applying the oblique shock relations, which are also available in standard compressible flow texts such as Reference 9.

2. ESTIMATION OF THE ROLL DAMPING OF A KE FIN

One approach to estimating the roll damping of a KE fin is to use a strip theory approach, breaking the fin planform into chordwise strips. Each strip is assumed to be a two-dimensional flat plate at angle of attack, where the local angle of attack is a function of the local circumferential velocity due to the spin and the axial component of the velocity. The roll moment is then determined by integrating the lift on each strip multiplied by the local moment arm. The roll damping moment, which is the variation in the roll moment with spin, can be determined by dividing the roll moment by the non-dimensional spin rate, since roll moment on the flat plate fin will be zero at zero spin rate. This assumes that the beveled trailing edge has little effect on the roll damping. This is consistent with the linearized potential theory

applied in the context of the spinning KE penetrator, which separates the trailing edge deflection effect (roll producing) from the angle of attack effects (roll damping).

From linearized potential theory,⁹ the lift coefficient on a two-dimensional flat plate at angle of attack may be expressed as follows

$$C_L = \frac{4\alpha}{\sqrt{M_\infty^2 - 1}} \quad (8)$$

By assuming that the flow conditions in front of the fins are approximately free stream, the lift on the strip can be written,

$$L = \frac{4\alpha(r)}{\sqrt{M_\infty^2 - 1}} \frac{1}{2} \rho_\infty M_\infty^2 a_\infty^2 c(r) \quad (9)$$

where $c(r)$ and $\alpha(r)$ are the local chord length and angle of attack respectively.

The roll moment coefficient is obtained by integrating the product of the lift and the moment arm, and non-dimensionalizing appropriately.

$$C_{\ell} = \frac{16N_{fins}}{\pi\sqrt{M_\infty^2 - 1}} \int_{r/D}^{r_2/D} \frac{c(r)}{D} \alpha\left(\frac{r}{D}\right) \frac{r}{D} d\left(\frac{r}{D}\right) \quad (10)$$

The local angle of attack can be approximated as follows,

$$\alpha\left(\frac{r}{D}\right) = \frac{pD}{V} \left(\frac{r}{D}\right) \quad (11)$$

The roll damping coefficient is obtained by dividing the roll moment coefficient by the non-dimensional spin rate.

IV. RESULTS

Computations have been performed to determine the following aerodynamic parameters which influence the roll characteristics of kinetic energy penetrators: the roll producing moment; the roll damping moment; and the equilibrium spin rate. Viscous computations were performed over a range of Mach numbers ($M = 3.0$ to 4.5) and spin rates ($pD/V = 0.$ to $pD/V = 0.0964$) for free-flight (sea-level) atmospheric conditions. Inviscid computations were performed to supplement the viscous computational results at zero spin rate. Unless otherwise noted, the computational results discussed below refer to those obtained using the viscous PNS procedure.

1. ROLL PRODUCING MOMENT

Figure 3 shows the development of the computed roll producing moment coefficient as a function of the axial position along the body at Mach 3 and zero spin rate. The computational result shows that for the M735 geometry, the roll producing moment is produced almost entirely by the fin asymmetries at the fin trailing edge and that the fin asymmetries at the fin leading edge contribute very little towards producing a roll moment. This is consistent with the estimates of the roll producing moment obtained using the engineering approach.

Figure 4 shows the roll producing moment coefficient as a function of Mach number as predicted by both viscous and inviscid computation and by the engineering approach. The trend predicted by the computational and engineering approaches compare well, though the engineering approach predicts a roll moment 30 to 50 percent greater than in the viscous computation. The roll moment predicted by the inviscid computation ranges from 15 to 28 percent greater than the viscous result.

Figures 5a and 5b display the pressure difference across the fin (from one side to the other) in the vicinity of the trailing edge as a function of the distance from the leading edge. This pressure difference is the mechanism that causes the roll producing moment. Pressure profiles at seven span locations are shown. Section 1 is located at one-eighth of the distance between the fin root and the fin tip, while section 7 is located at seven-eighths of this distance. The other five sections are spaced equally in-between as shown in Figure 6. Figures 5a and 5b display the inviscid and viscous results, respectively. A reference value corresponding to the pressure drop across a two-dimensional wedge is also plotted on both of these figures.

Both sets of results show that in front of the trailing edge chamfer, the magnitude of the pressure difference is nearly zero, but rises sharply on the trailing edge chamfer. The inviscid results attain the reference value except at positions near the tip of the fin. The viscous results approach the reference value in a more asymptotic manner due to the presence of the boundary layer. In the viscous results, tip effects also produce a smaller pressure differential at section 7. The viscous results also show a slightly smaller pressure differential at section 1. This can be attributed to the thick boundary layer on the cylindrical portion of the body. The thickness of this boundary layer can be seen in Figure 7, which shows the Mach number contours at an axial station in the vicinity of the trailing edge.

These detailed pressure profiles help explain the differences between roll producing moments predicted by the viscous, inviscid, and engineering estimates. The inviscid roll producing moment is larger than the viscous roll producing moment because the effect of the body and fin boundary layers on the driving pressure difference is neglected, due to the inviscid assumption. The engineering estimate, which assumes that the pressure difference across the trailing edge chamfer is the reference value, over-estimates the roll producing moment because tip effects as well as viscous effects are completely ignored.

2. ROLL MOMENT ON A SPINNING PROJECTILE

For each Mach number, computation of the flow field over the body has been performed for a number of fixed spin rates. The direction of spin is in the same direction as the zero-spin roll moment.

Figure 8 displays the development of the net roll moment coefficient over the projectile at a flight velocity of Mach 3 and rolling at a non-dimensional spin rate of .008568 (40 rps). This figure shows that relatively little roll damping is produced by the axisymmetric portion of the body. Once on the fin, the net roll moment shows an initial rapid decrease as a result of the roll damping contribution which opposes the spin. Near the aft end of the projectile, the net roll moment begins to increase as the roll producing moment predominates over the roll damping contribution. For the particular spin rate shown here, the total net roll moment is positive, indicating that the equilibrium spin rate will be greater than this particular spin rate.

The computed net roll moment coefficient as a function of spin rate at Mach 3.0 is shown in Figure 9. Clearly shown is the decrease in net roll moment with spin rate. This decrease is due to the increase in the roll damping contribution of the net roll moment as the spin rate increases. The results confirm that net roll moment varies linearly with spin rate, as discussed previously.

The slope of curve shown in Figure 9 represents the roll damping for this Mach number. Similar computations have been performed at the other Mach numbers and the roll damping computed for each of these Mach numbers. The computed roll damping coefficient as a function of Mach number is shown in Figure 10. Also shown is the roll damping coefficient as predicted using the engineering estimate. The engineering estimate predicts a roll damping coefficient which is 28 to 34 percent greater than the computation, though the trend of both predictions is consistent.

Figure 9 also shows that at Mach 3, the equilibrium spin rate, (the spin rate at which the net roll moment becomes zero) occurs at a non-dimensional spin rate of .00908, corresponding to 42.4 revolutions per second. The non-dimensional equilibrium spin rate as a function of Mach number is shown in Figure 11. Equilibrium spin rates obtained from the engineering approach are also shown in this figure. Differences of up to seventeen percent between the two approaches are observed. The computational results show less variation of the dimensional equilibrium spin rate with Mach number than does the engineering estimation, as shown in Figure 12.

3. TRAJECTORY SIMULATION

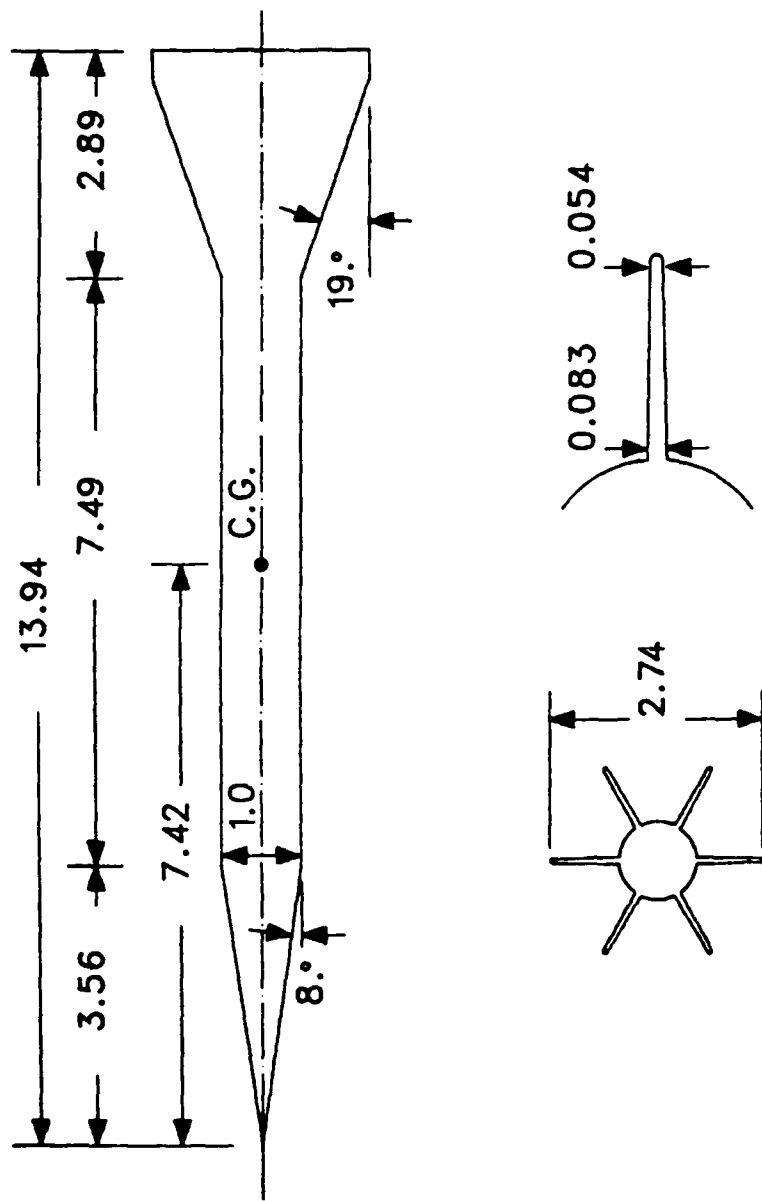
The roll history of the projectile has been computed by solving Equations (1) and (2). The effect of the projectile deceleration due to drag (65 km/sec per kilometer) has been considered. Roll histories have been obtained using both the computed roll coefficients and the coefficients obtained using the engineering approach. The roll histories were obtained for a launch velocity of Mach 4.25, atmospheric conditions, and zero initial roll rate. The results, shown in Figure 13, show a rapid spin-up over the first half kilometer of flight, followed by a slow decrease in spin rate over the rest of the trajectory. Both trajectories are similar, though the results obtained using

the engineering estimated coefficients show a slightly higher spin rate throughout the trajectory. The results also show that, after about 0.75 kilometers, the projectile is flying at the equilibrium spin rate where the spin rate is just a function of the local Mach number. This is shown in Figure 14, where the equilibrium spin rate and the spin rate from the trajectory simulation as a function of Mach number are displayed. The results show that after the initial spin-up transient, the projectile is flying at the equilibrium spin rate.

V. CONCLUSION

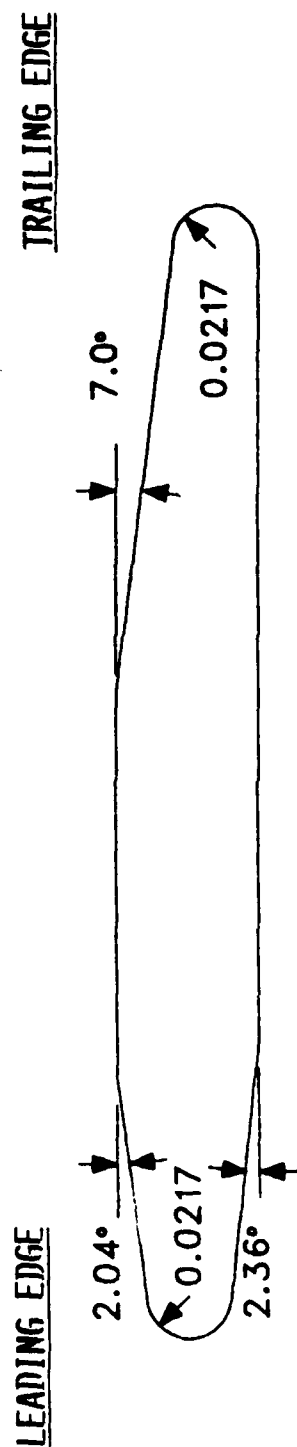
The roll characteristics (roll producing moment, roll damping moment, and equilibrium spin rate) of a kinetic energy penetrator have been obtained using Computational Fluid Dynamics techniques. The computed results show that viscous computation is required to compute the roll characteristics accurately, based on the differences between the viscous and inviscid results.

The computational results have been used to benchmark engineering approaches for estimating these roll characteristics. For the particular projectile examined here, the engineering approaches over-estimated the roll producing moment by up to 50 percent and the roll damping moment by as much as 34 percent, though the trend predicted by computation and engineering estimation is similar. The predicted values of equilibrium spin rate differ by a maximum of 17 percent, though the computed results show a greater variation with Mach number than do the values determined from the engineering estimation approach.



ALL DIMENSIONS IN CALIBERS (ONE CALIBER = 35.2 mm)

Figure 1. Schematic of M735 Finned Projectile Geometry.



ALL DIMENSIONS IN CALIBERS (ONE CALIBER = 35.2 mm)

Figure 2. Schematic of M735 Fin Cross-Sectional Geometry.

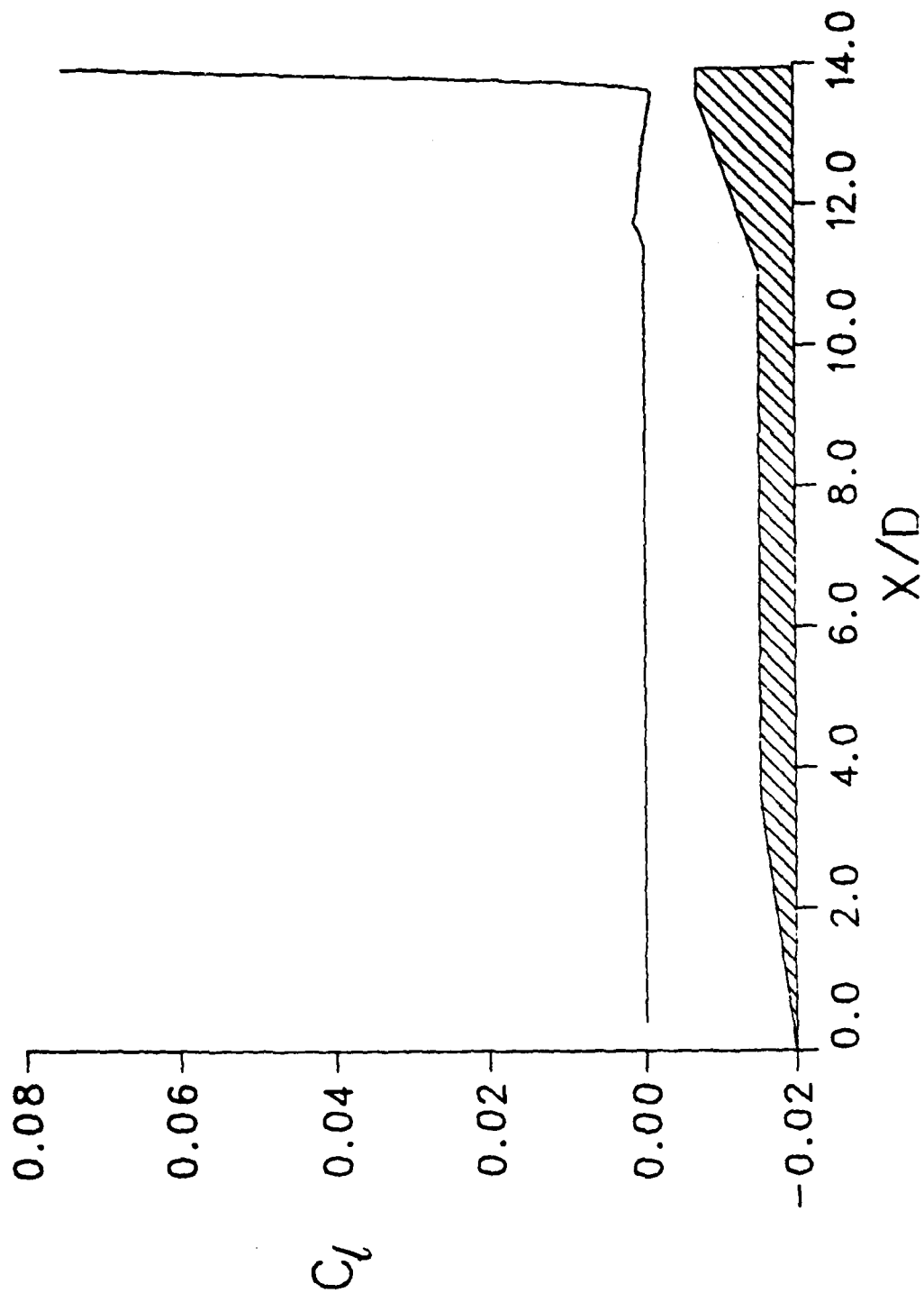


Figure 3. Development of Roll Producing Moment Coefficient with Axial Position, $M = 3$, $pd/V = 0$.

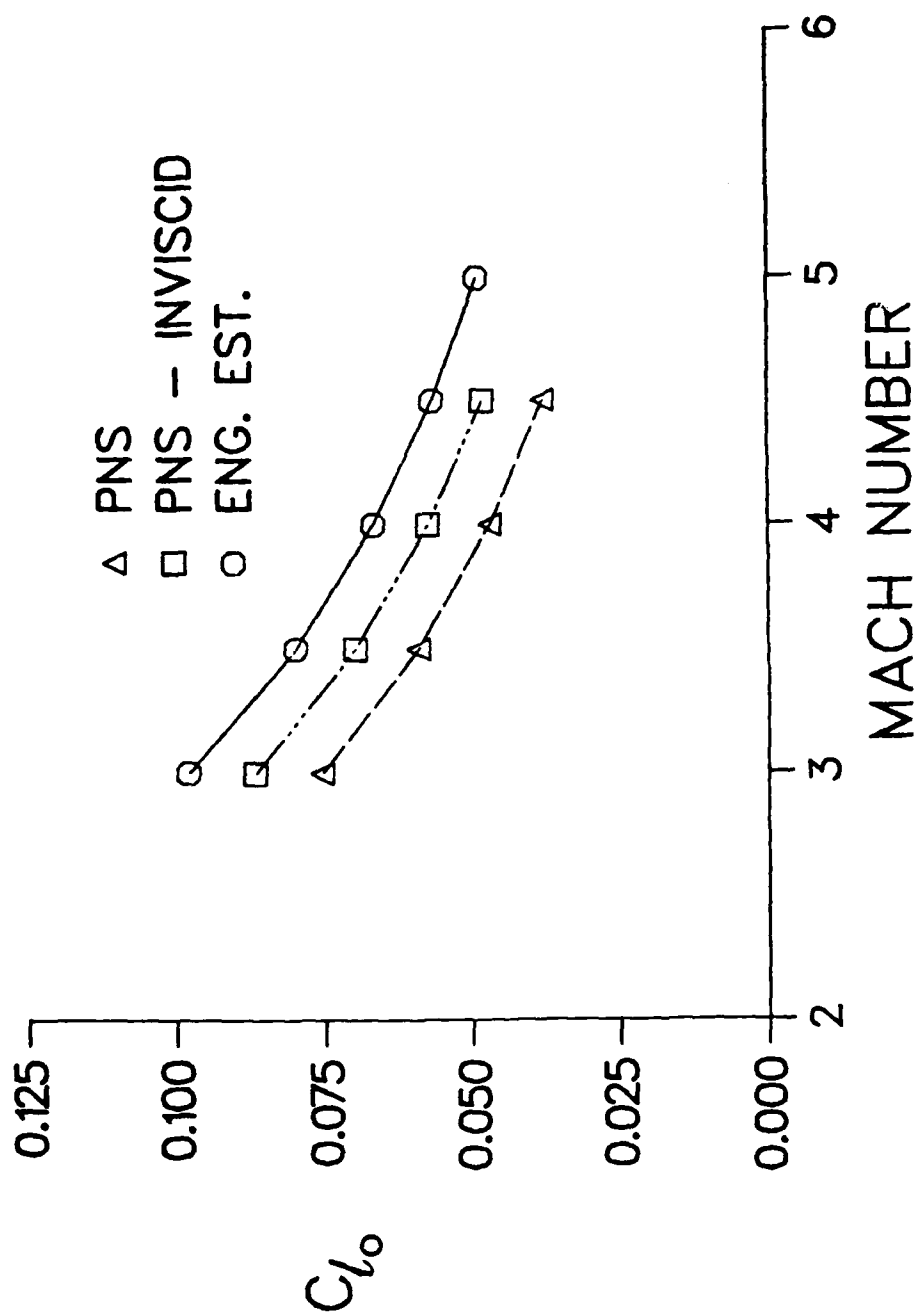


Figure 4. Variation of Roll Producing Moment Coefficient with Mach Number.

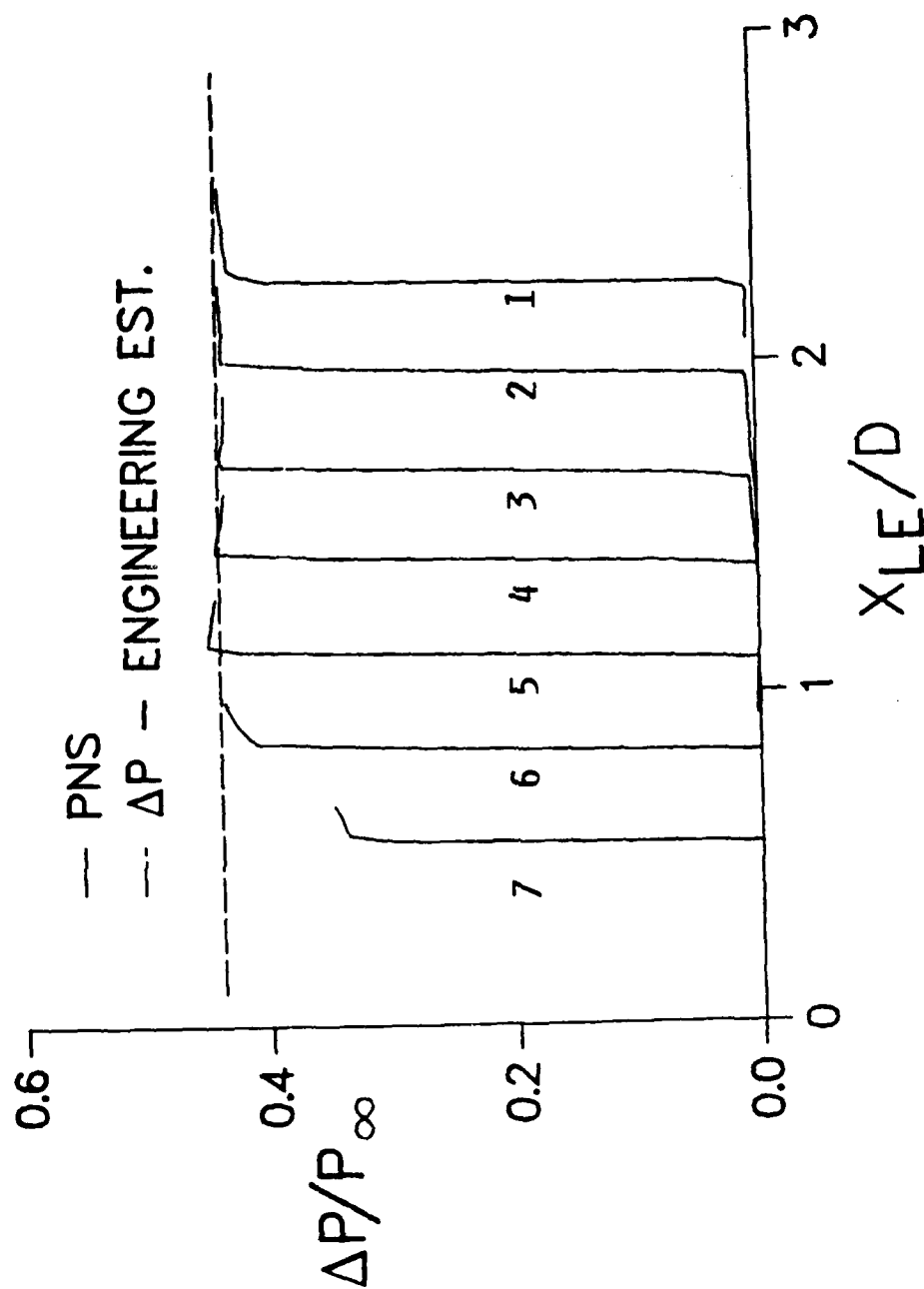


Figure 5a. Pressure Difference Across Fin Near Trailing Edge, Sections 1-7, Inviscid Result.

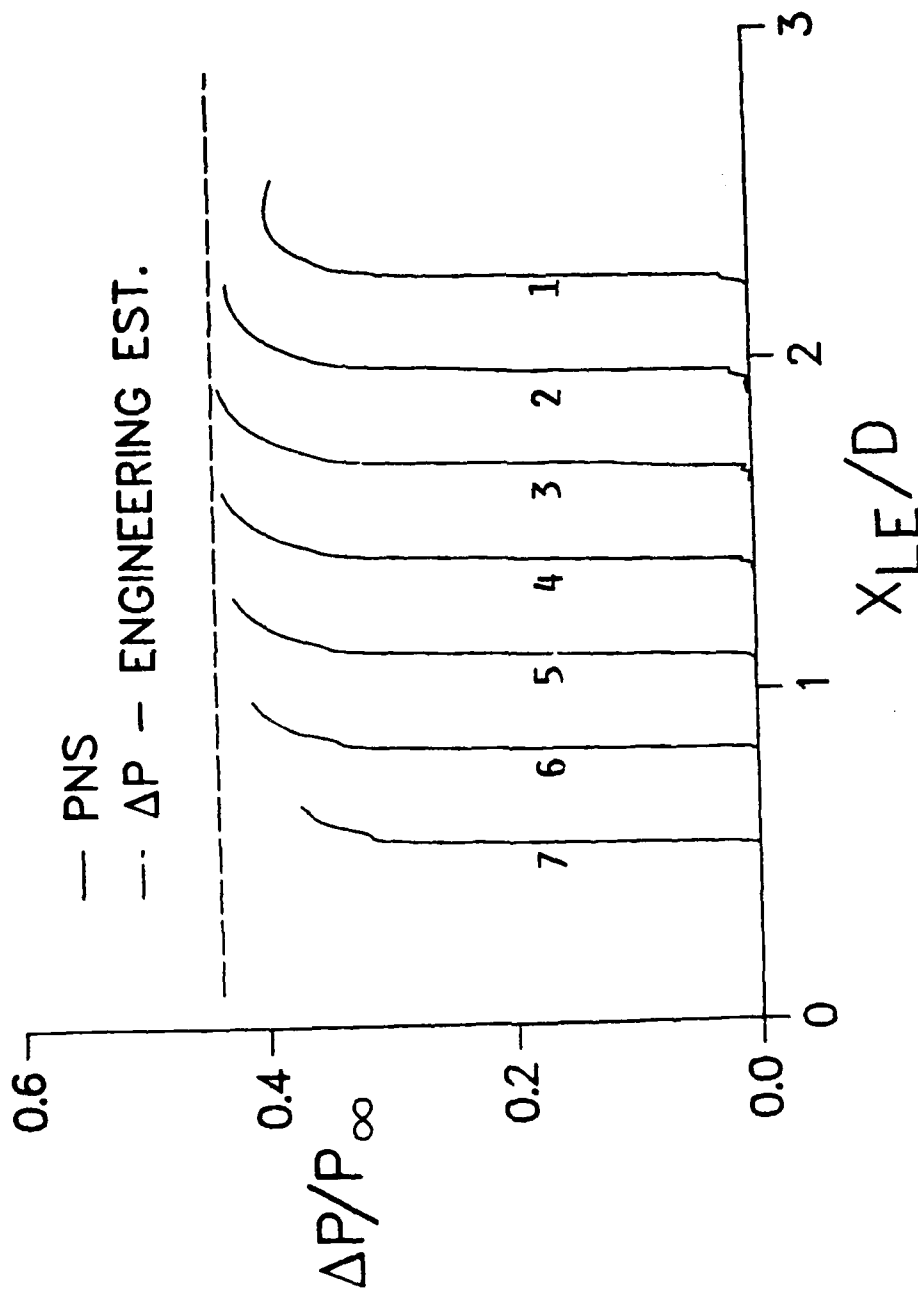


Figure 5b. Pressure Difference Across Fin Near Trailing Edge, Sections 1-7, Viscous Result.

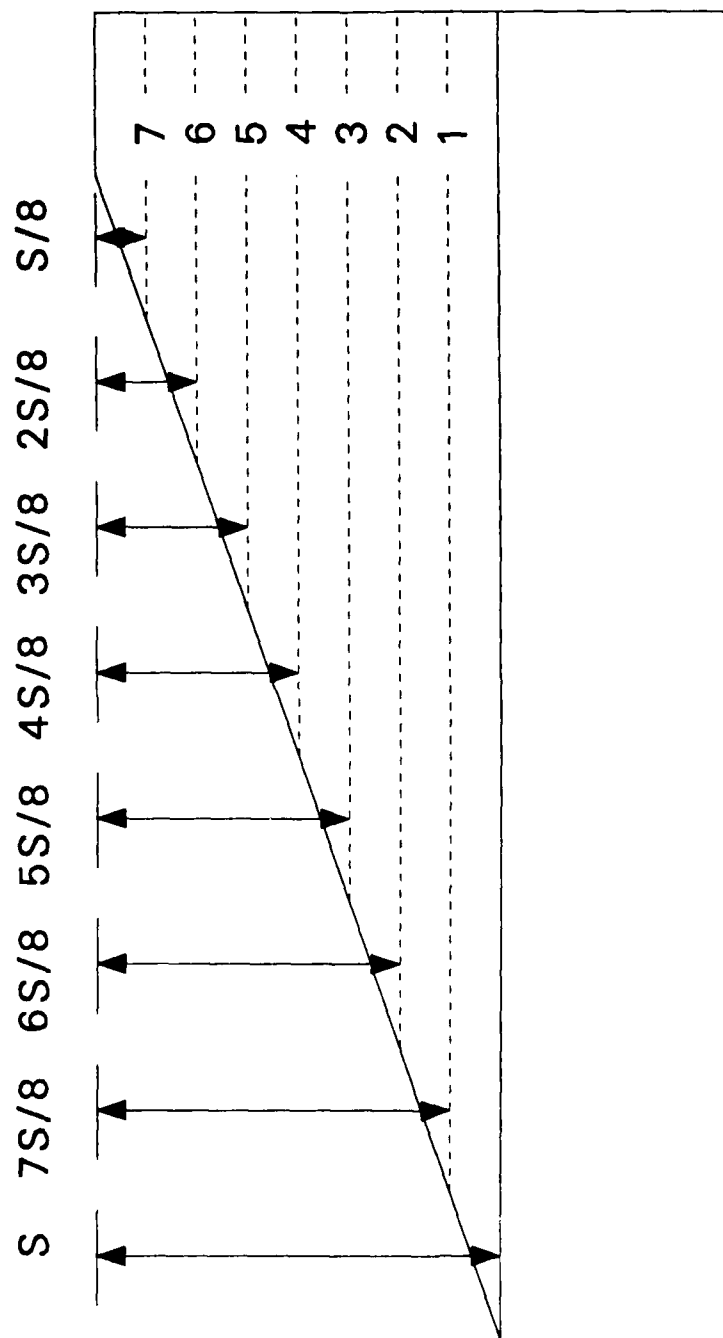


Figure 6. Schematic Showing Spanwise Location of Pressure Profiles.

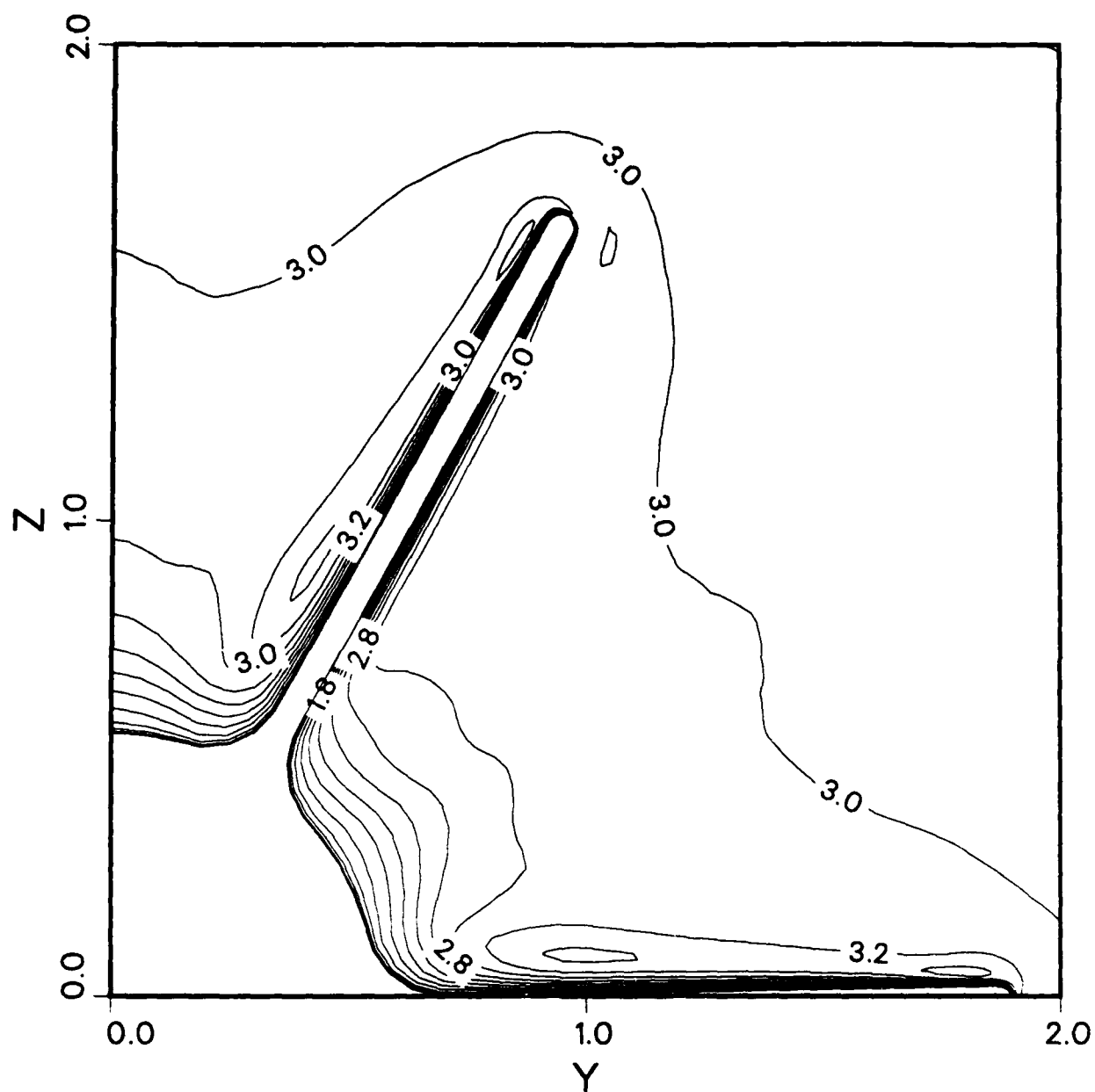


Figure 7. Mach Contours in Vicinity of Trailing Edge, $M = 3$, $p_0/V = 0$.

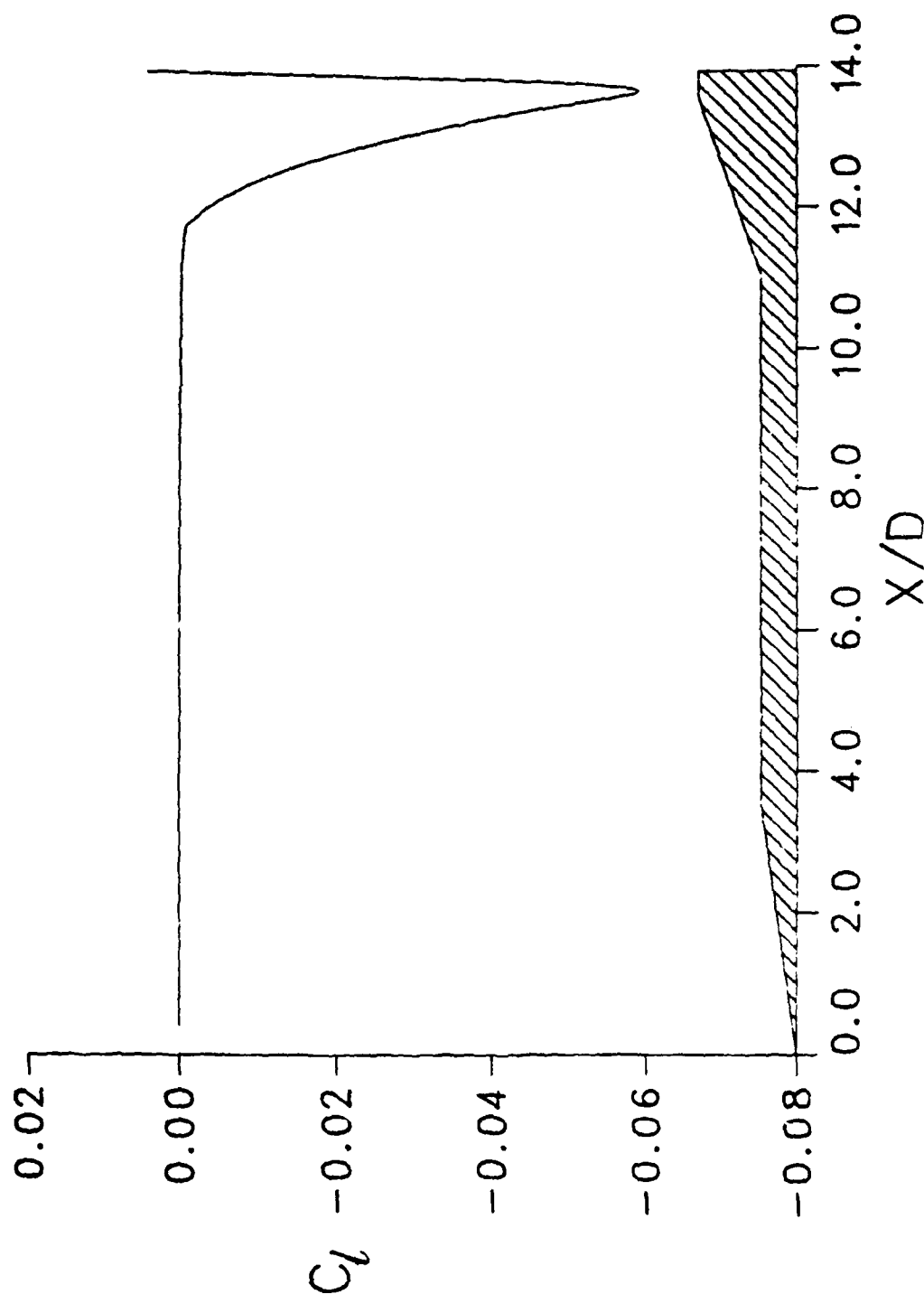


Figure 8. Development of Net Roll Moment Coefficient with Axial Position, $M = 3$, $pD/V = 0.008568$.

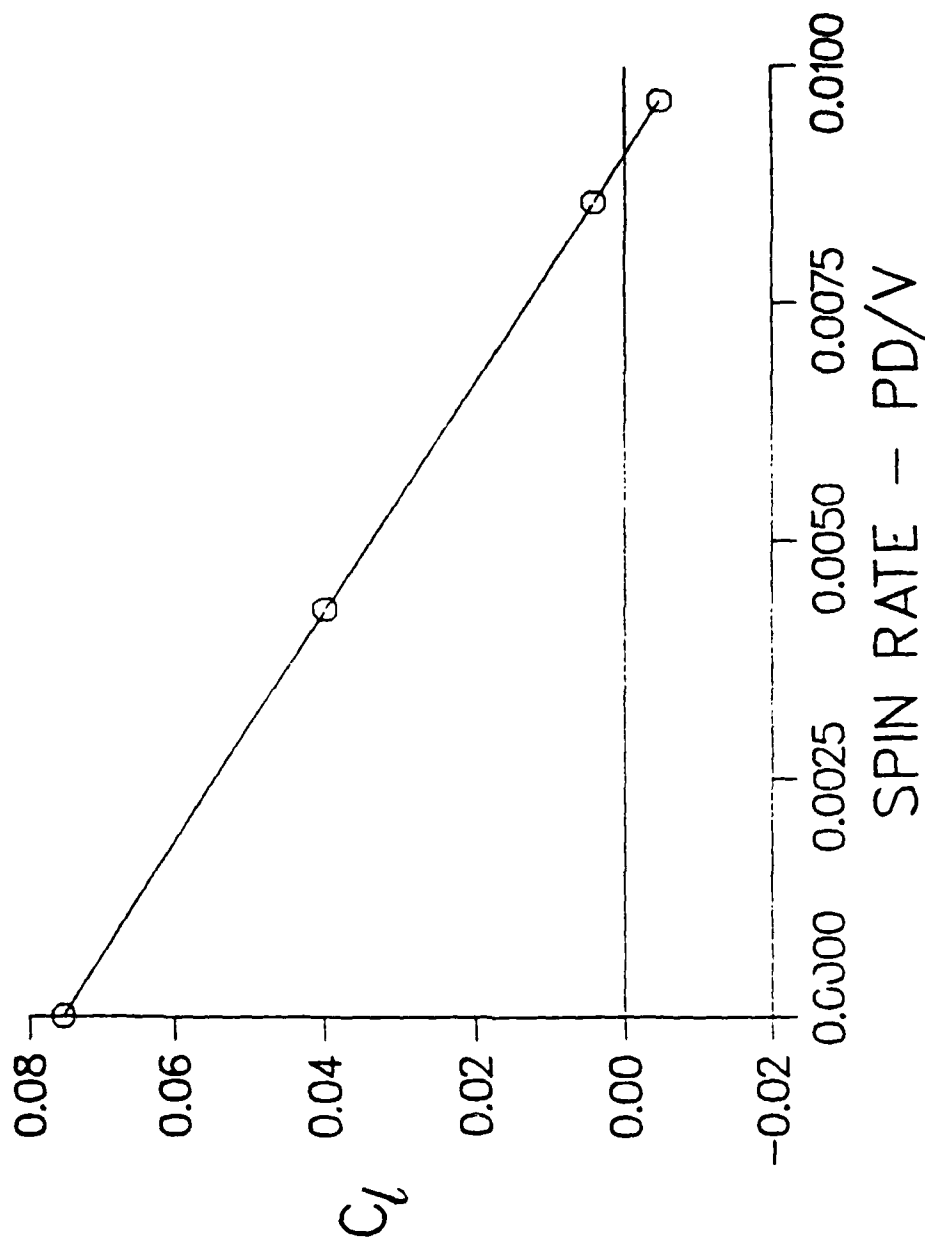


Figure 9. Variation of Net Roll Moment Coefficient with Spin Rate, $M = 3.0$.

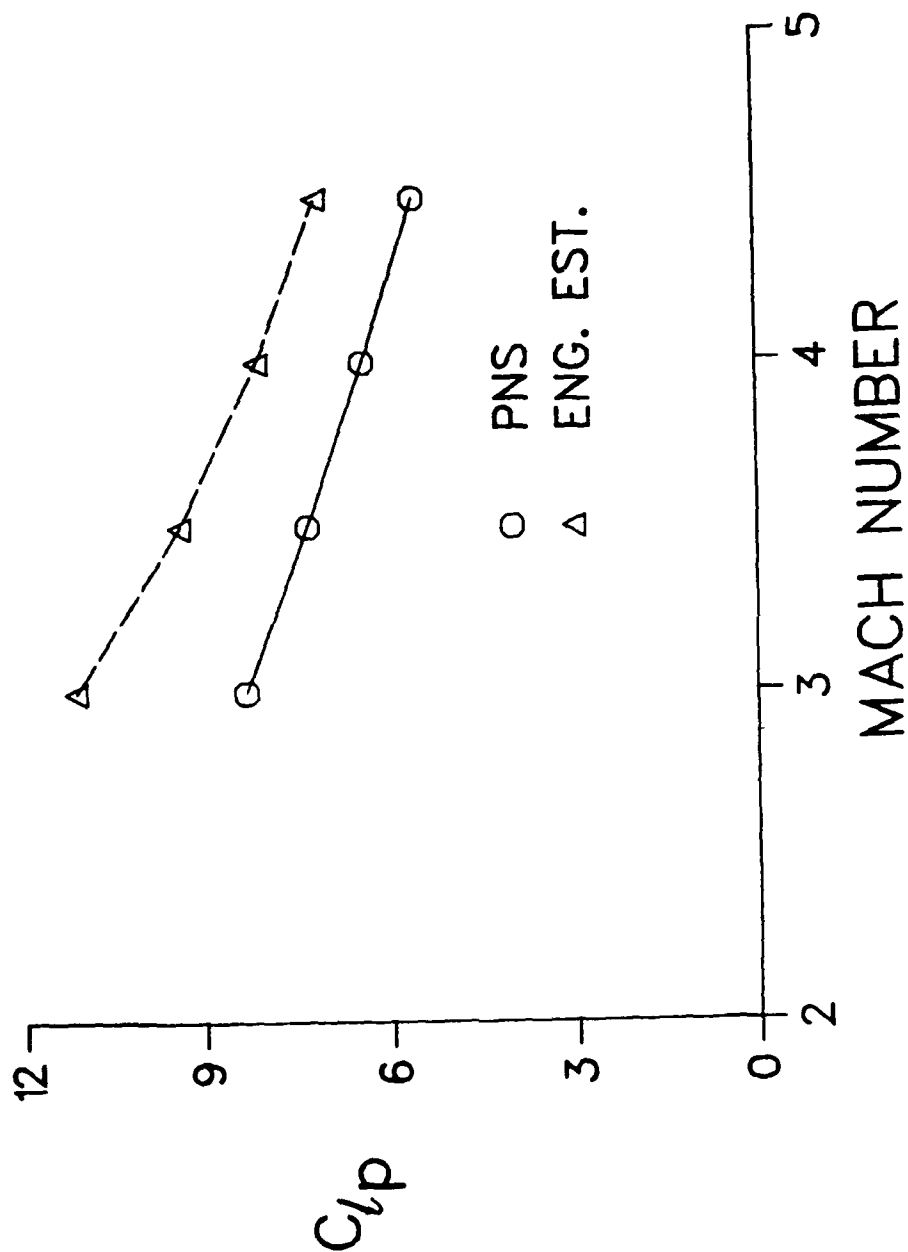


Figure 10. Variation of C_{dp} Damping Coefficient with Mach Number.

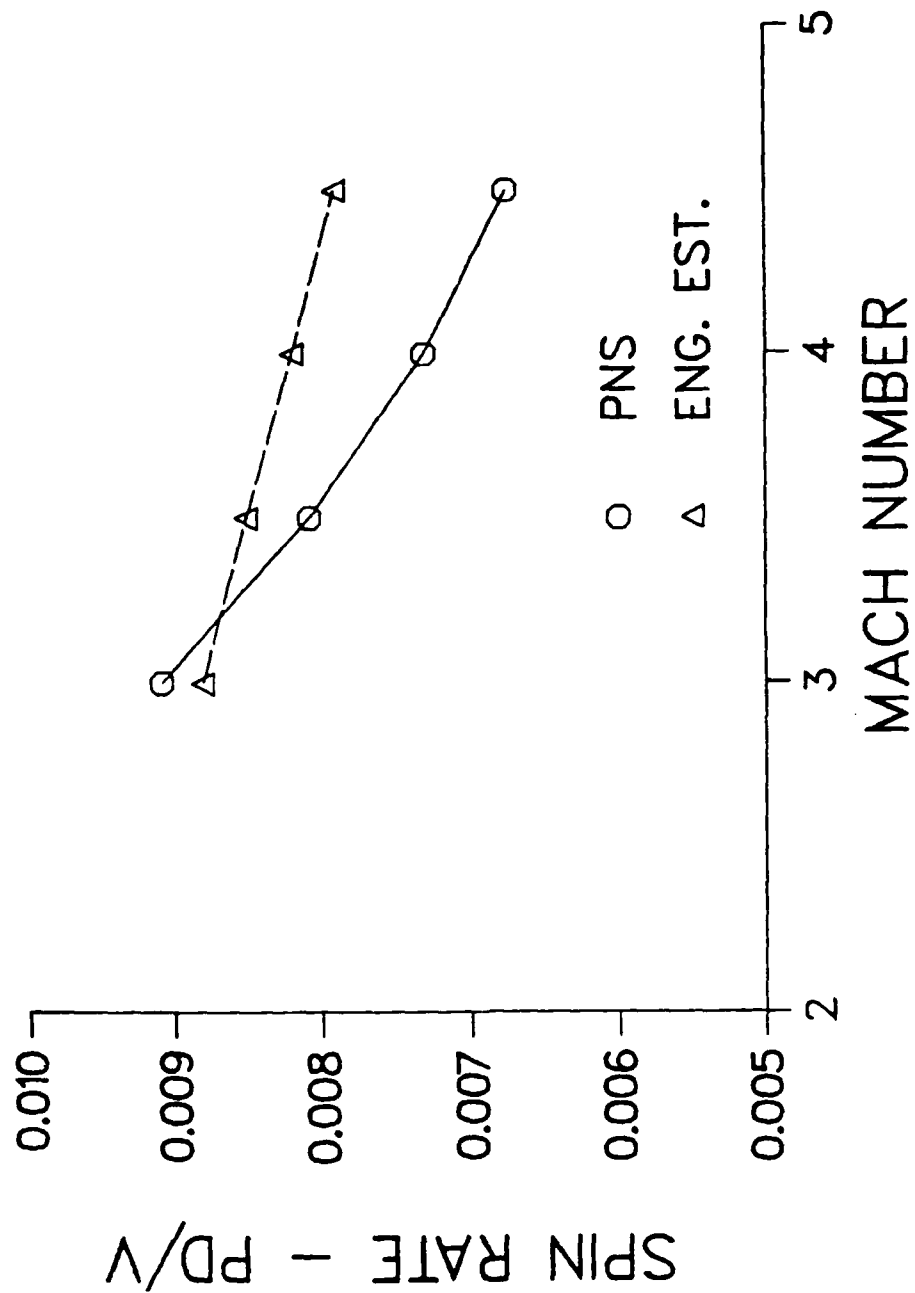


Figure 11. Variation of Non-dimensional Equilibrium Spin Rate with Mach Number.

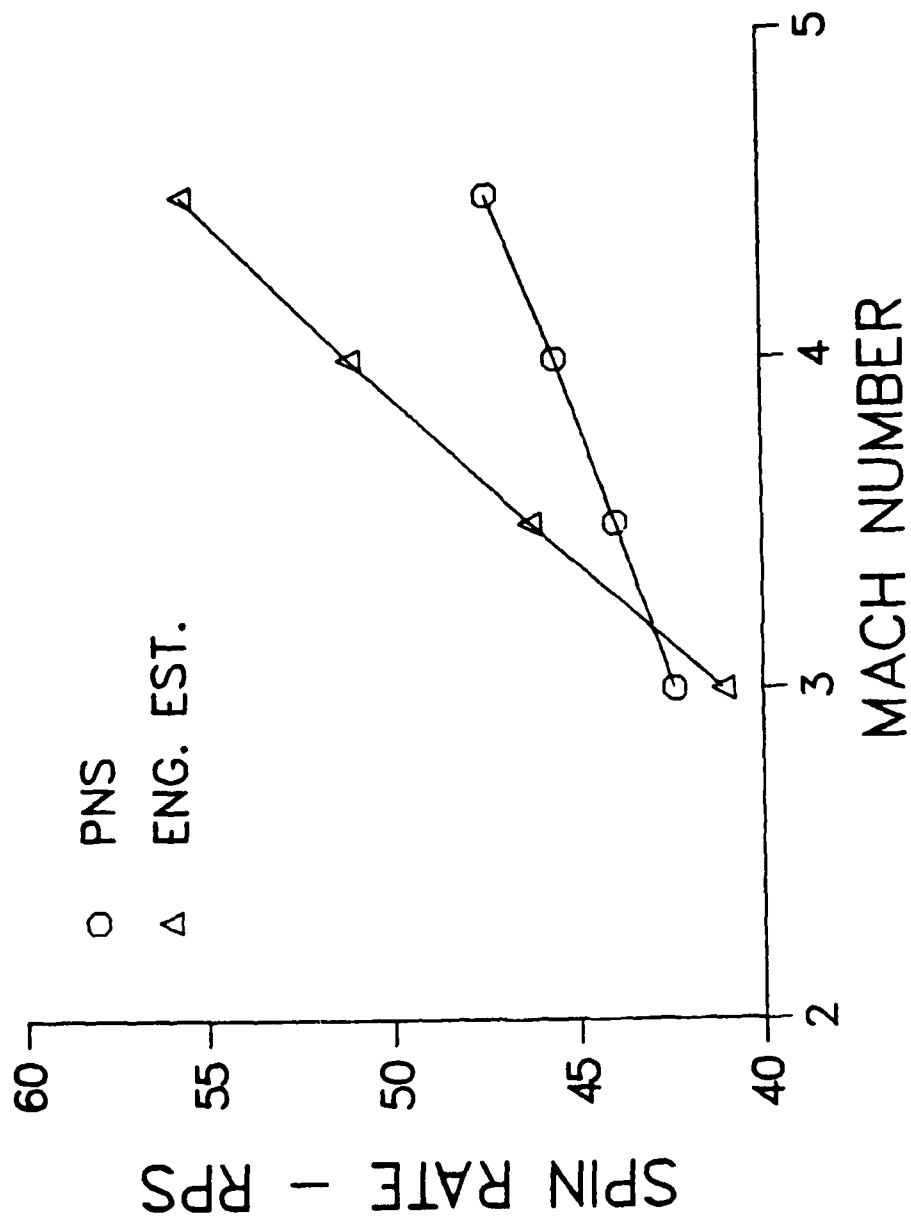


Figure 12. Variation of Dimensional Equilibrium Spin Rate with Mach Number.

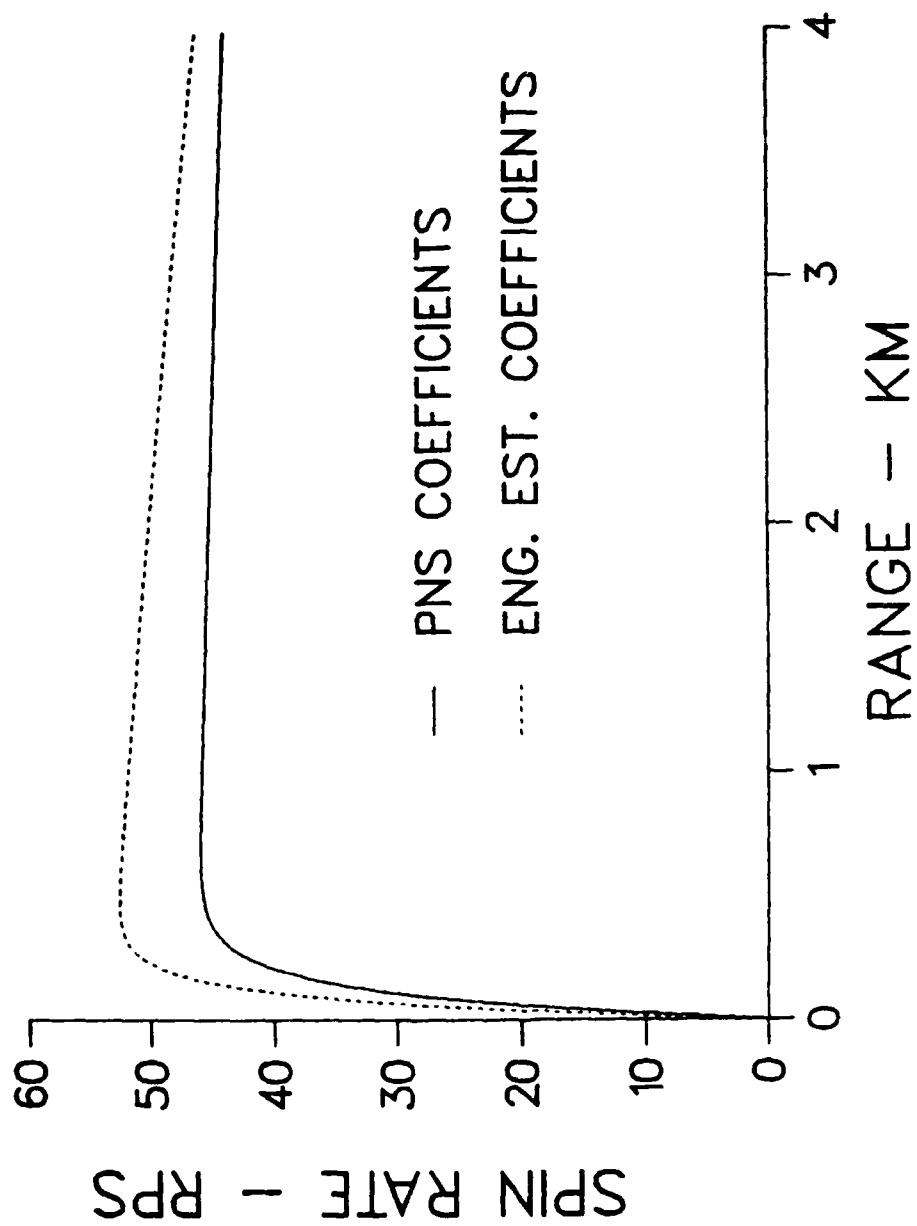


Figure 13. Roll rate history from trajectory simulation using computed and estimated roll coefficients.

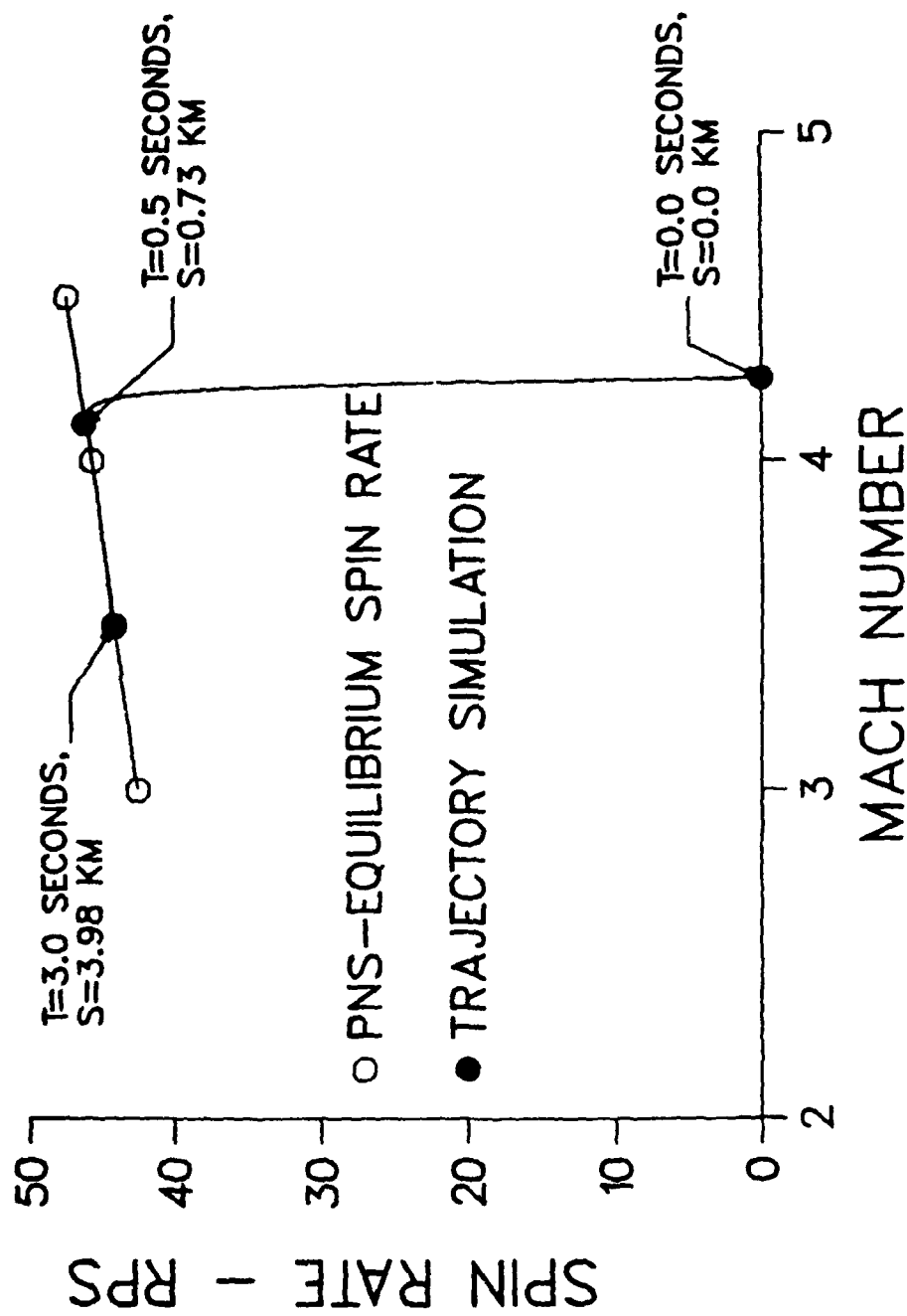


Figure 14. Comparison of spin rate versus Mach number for equilibrium spin rate and trajectory simulation.

REFERENCES

1. Sturek, W.B. and Schiff, L.B., "Numerical Simulation of Steady Supersonic Flow over Spinning Bodies of Revolution," AIAA Journal, Vol. 20, No. 12, December 1982, pp 1724-1731.
2. Sturek, W.B. and Mylin, D.C., "Computational Parametric Study of the Magnus Effect on Boattailed Shell at Supersonic Speeds," AIAA Paper 81-1900, 8th Atmospheric Flight Mechanics Conference, August 1981.
3. Weinacht, P., Guidos, B.J. and Sturek, W.B., "PNS Computations for Spinning and Fin-Stabilized Projectiles at Supersonic Velocities," U.S. Army Ballistic Research Laboratory, Aberdeen Proving Ground, Maryland, ARBRL-MR-03464, September 1985. (AD A160393)
4. Weinacht, P., Guidos, B.J., Sturek, W.B. and Hodes, B.A., "PNS Computations for Spinning Shell at Moderate Angles of Attack and for Long L/D Finned Projectiles," U.S. Army Ballistic Research Laboratory, Aberdeen Proving Ground, Maryland, ARBRL-MR-03522, June 1986.
5. Murphy, C.H., "Free Flight Motion of Symmetric Missiles," U.S. Army Ballistic Research Laboratory, Aberdeen Proving Ground, Maryland, Report No. 1216, July 1963. (AD A442757)
6. Baldwin, B.S. and Lomax, H., "Thin Layer Approximation and Algebraic Model for Separated Turbulent Flows," AIAA Paper 78-257, 16th Aerospace Sciences Meeting, January 1978.
7. Schiff, L.B. and Steger, J.L., "Numerical Simulation of Steady Supersonic Viscous Flow," AIAA Journal, Vol. 18, No. 12, December 1980, pp. 1421-1430.
8. Beam, R. and Warming, R.F., "An Implicit Factored Scheme for the Compressible Navier-Stokes Equations," AIAA Journal, Vol. 16, No. 4, 1978, pp. 85-129
9. John, J.E.A., "Gas Dynamics", Boston, Allyn and Bacon, 1969.

LIST OF SYMBOLS

a_{∞}	freestream speed of sound
A	area of trailing edge chamfer
A_R, A_L	area of right and left side of leading edge chamfer
$c(r)$	local chord length of fin
C_{ℓ}	roll moment coefficient
C_{ℓ_0}	roll producing moment coefficient
C_{ℓ_p}	roll damping moment coefficient
C_L	lift coefficient
D	projectile diameter
e	total energy per unit volume
E, F, G	flux vectors in transformed coordinates
G_v	viscous flux vector in transformed coordinates
H	source term resulting from rotating coordinate frame
I	moment of inertial
J	Jacobian
L	lift
M	Mach number
M_{∞}	freestream Mach number
N_{fins}	number of fins
p	spin rate
$\frac{pD}{v}$	nondimensional spin rate
P	pressure
P_{∞}	freestream static pressure
Pr	Prandtl number

Pr_t	turbulent Prandtl number
P_R, P_L	pressure on right and left side of leading edge chamfer
r	radial coordinate
S	inviscid source term resulting from the cylindrical coordinate formulation
S_{ref}	reference cross sectional area of projectile
S_v	viscous source term resulting from cylindrical coordinate formulation
t	time
u, v, w	axial, tangential, and normal velocity components of the Navier-Stokes equations
U, V, W	Contravariant velocities of the transformed Navier-Stokes equations
V	freestream velocity used to non-dimensionalize the spin rate and the aerodynamic coefficients
x_{LE}	distance from fin leading edge
y_R, y_L	distance from projectile axis to centroid of area of leading edge chamfer on the left and right side of fin
z	distance from projectile axis to centroid of area of trailing edge chamfer

Greek Symbols

$\alpha(r)$	local angle of attack
γ	ratio of specific heats
ΔP	pressure difference across fin
μ	molecular viscosity
μ_t	turbulent viscosity
ξ, η, ζ	transformed coordinates
ρ	density
ρ_∞	freestream density
Ω	spin rate of projectile

DISTRIBUTION LIST

<u>No. of Copies</u>	<u>Organization</u>	<u>No. of Copies</u>	<u>Organization</u>
12	Administrator Defense Technical Info Center ATTN: DTIC-FDAC Cameron Station, Bldg. 5 Alexandria, VA 22304-6145	1	Commander US Army Armament, Munitions and Chemical Command ATTN: AMSMC-IMP-L Rock Island, IL 61299-7300
1	HQDA DAMA-ART-M Washington, DC 20310	1	Commander US Army Aviation Systems Command ATTN: AMSAV-ES 4300 Goodfellow Blvd St. Louis, MO 63120-1798
1	Commander US Army Materiel Command ATTN: AMCDRA-ST 5001 Eisenhower Avenue Alexandria, VA 22333-0001	1	Director US Army Aviation Research and Technology Activity Ames Research Center Moffett Field, CA 94035-1099
1	Commander US Army Armament Research, Development and Engineering Center ATTN: SMCAR-MSI Dover, NJ 07801-5001	10	C.I.A. OIR/DB/Standard GE47 HQ Washington, DC 20505
1	Commander US Army Armament Research, Development and Engineering Center ATTN: SMCAR-TDC Dover, NJ 07801-5001	1	Commander US Army Communications - Electronics Command ATTN: AMSEL-ED Fort Monmouth, NJ 07703-5301
5	Commander US Army Armament Research, Development and Engineering Center ATTN: SMCAR-TSS SMCAR-LCA-F, R. Kline S. Kahn H. Hudgins J. Grau Dover, NJ 07801-5001	1	Commander CECOM R&D Technical Library ATTN: AMSEL-IM-L (Reports Section) B. 2700 Fort Monmouth, NJ 07703-5000
		3	Commander US Army Missile Command Research, Development and Engineering Center ATTN: AMSMI-RD Redstone Arsenal, AL 35898-5230
1	Commander US AMCCOM ARDEC CCAC Benet Weapons Laboratory ATTN: SMCAR-CCB-TL Watervliet, NY 12189-4050	1	Director US Army Missile and Space Intelligence Center ATTN: AIAMS-YDL Redstone Arsenal, AL 35898-5500

DISTRIBUTION LIST

<u>No. of Copies</u>	<u>Organization</u>	<u>No. of Copies</u>	<u>Organization</u>
1	Commander US Army Tank Automotive Command ATTN: AMSTA-TSL Warren, MI 48397-5000	1	Director National Aeronautics and Space Administration Langley Research Center ATTN: Tech Library Langley Station Hampton, VA 23365
2	Commander Naval Surface Weapons Center ATTN: Code R44 (Dr. F. Priolo) (Dr. A. Wardlaw) K-24, Building 402-12 White Oak Laboratory Silver Spring, MD 20903-5000	5	Director National Aeronautics and Space Administration Ames Research Center ATTN: MS-227-8, L. Schiff MS-258-1, J. Steger D. Chaussee M. Rai J. Cordova Moffett Field, CA 94035
1	Commander US Naval Surface Weapons Center ATTN: Dr. F. Moore Dahlgren, VA 22448	1	Air Force Armament Laboratory ATTN: AFATL/FXA (Stephen C. Korn) Eglin AFB, FL 32542-5434
1	Director US Army TRADOC Analysis Center ATTN: ATOR-TSL White Sands Missile Range, NM 88002-5502	1	Massachusetts Institute of Technology ATTN: Tech Library 77 Massachusetts Avenue Cambridge, MA 02139
1	Commandant US Army Infantry School ATTN: ATSH-CD-CS-OR Fort Benning, GA 31905-5400		
1	Commander US Army Development and Employment Agency ATTN: MODE-ORO Fort Lewis, WA 98433-5000		<u>Aberdeen Proving Ground</u> Dir, USAMSAA ATTN: AMXS-D AMXS-MP, H. Cohen
1	AFWL/SUL Kirtland AFB, NM 87117		Cdr, USATECOM ATTN: AMSTE-SI-F
1	Air Force Armament Laboratory ATTN: AFATL/DLODL (Tech Info Center) Eglin AFB, FL 32542-5000		Cdr, CRDC, AMCCOM, ATTN: SMCCR-RSP-A SMCCR-MU SMCCR-SPS-IL
2	Director Sandia National Laboratories ATTN: Dr. W. Oberkamp Dr. F. Blottner Division 1636 Albuquerque, NM 87185		

USER EVALUATION SHEET/CHANGE OF ADDRESS

This Laboratory undertakes a continuing effort to improve the quality of the reports it publishes. Your comments/answers to the items/questions below will aid us in our efforts.

1. BRL Report Number _____ Date of Report _____
2. Date Report Received _____
3. Does this report satisfy a need? (Comment on purpose, related project, or other area of interest for which the report will be used.) _____

4. How specifically, is the report being used? (Information source, design data, procedure, source of ideas, etc.) _____

5. Has the information in this report led to any quantitative savings as far as man-hours or dollars saved, operating costs avoided or efficiencies achieved, etc? If so, please elaborate. _____

6. General Comments. What do you think should be changed to improve future reports? (Indicate changes to organization, technical content, format, etc.) _____

CURRENT ADDRESS

Name _____

Organization _____

Address _____

City, State, Zip _____

7. If indicating a Change of Address or Address Correction, please provide the New or Correct Address in Block 6 above and the Old or Incorrect address below.

OLD ADDRESS

Name _____

Organization _____

Address _____

City, State, Zip _____

(Remove this sheet, fold as indicated, staple or tape closed, and mail.)

----- FOLD HERE -----

Director
U.S. Army Ballistic Research Laboratory
ATTN: SLCBR-DD-T
Aberdeen Proving Ground, MD 21005-5066

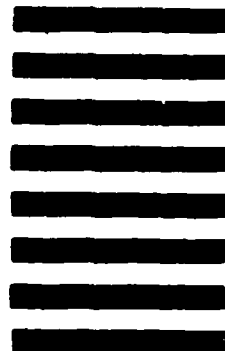


NO POSTAGE
NECESSARY
IF MAILED
IN THE
UNITED STATES

OFFICIAL BUSINESS
PENALTY FOR PRIVATE USE, \$300

BUSINESS REPLY MAIL
FIRST CLASS PERMIT NO 12062 WASHINGTON, DC
POSTAGE WILL BE PAID BY DEPARTMENT OF THE ARMY

Director
U.S. Army Ballistic Research Laboratory
ATTN: SLCBR-DD-T
Aberdeen Proving Ground, MD 21005-9989



----- FOLD HERE -----